

## Supplementary Information

### Graphene Quantum Dot Surface Passivation with Polymers for Two-Photon Properties under Two-Photon Excitation†

Wen-Shuo Kuo,<sup>\*‡abcd</sup> Chih-Li Lilian Hsu,<sup>‡e</sup> Hua-Han Chen,<sup>‡f</sup> Chia-Yuan Chang,<sup>cd</sup> Hui-Fang Kao,<sup>g</sup> Lawrence Chao-Shan Chou,<sup>c</sup> Yi-Chun Chen,<sup>h</sup> Shean-Jen Chen,<sup>ad</sup> Wen-Tsan Chang,<sup>i</sup> Shih-Wen Tseng,<sup>c</sup> Jiu-Yao Wang<sup>\*b,e,i</sup> and Ying-Chih Pu<sup>\*j</sup>

<sup>a</sup>Advanced Optoelectronic Technology Center, National Cheng Kung University, Tainan 701, Taiwan (R.O.C.).

<sup>b</sup>Allergy & Clinical Immunology Research Center, National Cheng Kung University, Tainan 701, Taiwan (R.O.C.).

<sup>c</sup>Center for Micro/Nano Science and Technology, National Cheng Kung University, Tainan 701, Taiwan (R.O.C.).

<sup>d</sup>College of Photonics, National Chiao Tung University, Tainan 711, Taiwan (R.O.C.).

<sup>e</sup>Department of Microbiology & Immunology, National Cheng Kung University, Tainan 701, Taiwan (R.O.C.).

<sup>f</sup>Department of Food Science, National Penghu University of Science and Technology, Penghu 880, Taiwan (R.O.C.).

<sup>g</sup>Department of Nursing, National Tainan Junior College of Nursing, Tainan 700, Taiwan (R.O.C.).

<sup>h</sup>Department of Physics, National Cheng Kung University, Tainan 701, Taiwan (R.O.C.).

<sup>i</sup>Department of Biochemistry and Molecular Biology, National Cheng Kung University, Tainan 701, Taiwan (R.O.C.).

<sup>j</sup>Department of Materials Science, National University of Tainan 700, Taiwan (R.O.C.).

\*To whom correspondence should be addressed. E-mail: wenshuokuo@mail.ncku.edu.tw (W. S. Kuo); a122@mail.ncku.edu.tw (J. Y. Wang); ycpu@mail.nutn.edu.tw (Y. C. Pu)

‡These authors contributed equally to this work.

## Experimental section

**Graphene quantum dot (GQD) preparation.** A modified Hummers method was used to prepare graphene oxide from the graphite (Bay carbon, SP-1, USA).<sup>1</sup> Graphite (8.5 M) and NaNO<sub>3</sub> (0.6 M) (Merck Germany) were mixed with H<sub>2</sub>SO<sub>4</sub> (18 M) (Wako, Japan). KMnO<sub>4</sub> (2.0 M) (J. T. Baker, USA) was slowly added and kept stirring at 35 °C overnight. Then, the ddH<sub>2</sub>O (1 Liter) was gradually added and kept stirred. The reaction was terminated by adding H<sub>2</sub>O<sub>2</sub> (35 wt %) (Shimakyu, Japan). Washing and centrifugation with ddH<sub>2</sub>O several times were addressed and the graphene oxide was collected. The as-prepared graphene oxide was heated to 400-600 °C in the presence of Argon for 4 h, and then were introduced to concentrated HNO<sub>3</sub> (16 M) (Wako, Japan) and stirred for 18h. The mixture was put in sonicator for at least 1 day and then put it in oven at 160 °C to vaporize all the liquid. Washing and centrifugation with ddH<sub>2</sub>O several times were addressed. The resulting black suspension was tuned the pH to 7.4 with NaOH (Merck Germany), and the GQDs were obtained.

**Synthesis and characterization of the GQD coated polymers (GQD@polymers) nanomaterials.** The positively charged polyoxyalkyleneamine (POAA) (100 µg mL<sup>-1</sup>) (HUNTSMAN, USA), positively charged poly(allylamine hydrochloride) (PAH) (100 µg mL<sup>-1</sup>) (Sigma-Aldrich Co., USA), negative charged poly(acrylic acid) (PAA) (Sigma-Aldrich Co., USA) and negative charged polystyrene sulfonate (PSS) (100 µg mL<sup>-1</sup>) (Sigma-Aldrich Co., USA) were coated on the surface of negative charged as-prepared GQD (100 µg mL<sup>-1</sup>) by the electrostatic interaction to form GQD@PAH, GQD@PAH@PAA, GQD@POAA, GQD@POAA@PAA and GQD@POAA@PSS, respectively. Centrifuging (80000 rpm) (Optima TLX Ultracentrifuge, BECKMAN, USA) the solutions for 15 min to remove nonspecific polymers. The pellets (GQD@polymer nanomaterials) were re-suspended in ddH<sub>2</sub>O, and the centrifugation process was repeated several times.

**Characterization.** Droplets of materials were allowed to dry on grids coated with Formvar. The materials were then subject to transmission electron microscopy (TEM, JEOL 1400, JEOL 2100, and JEOL 3010, Japan) observation. The height profile diagram, thickness and size of materials were determined by atomic force microscopy (AFM, multimode 8, Bruker, Germany). The crystalline structures of materials were identified using X-ray diffraction (XRD, Bruker AXS GmbH, Germany/ D2 Phaser) with CuK $\alpha$  radiation at 30 kv and 30 mA. Fourier transform infrared (FTIR), ultraviolet-visible (UV-vis), and zeta potential spectra of materials were recorded by the spectrometers : PerkinElmer RX1 USA, U-4100 Hitachi Japan and Manern Nano-ZS90 UK, respectively. Raman spectroscopy (DXR, Thermo Scientific, USA) was examined the crystallinity of materials with 532 nm laser. The photoluminescence (PL) signal was recorded by the spectrophotometer (F-7000,

Hitachi, Japan). X-ray photoelectron spectroscopy (XPS, PHI 5000, VersaProbe, USA) was examined the surface chemistry of materials.

**Cell culture for human lung carcinoma malignant cell line (A549 cell).** The cell culture of A549 cells was according to our published papers.<sup>2-4</sup>

**Quantum yield (QY) measurement.** The photoluminescence (PL) QY of contrast agent is the usually the ratio of the emitted photons to the absorbed photons. It can be led to

$$QY = QY_{\text{ref}} \frac{\eta^2}{\eta_{\text{ref}}^2} \frac{I}{A} \frac{A_{\text{ref}}}{I_{\text{ref}}} \quad (1)$$

, where  $QY_{\text{ref}} = 0.72$  is the QY of fluorescein dissolved in ddH<sub>2</sub>O (pH 11) as a reference,<sup>5,6</sup>  $\eta$  is the refractive index of ddH<sub>2</sub>O=1.3333,  $A$  is the absorbance of the excitation wavelength and  $I$  is the integrated fluorescence intensity. Results were showed in **Table 1**. One-photon excitation or two-photon excitation (TPE) yields the same QY.<sup>7</sup>

**Nonlinear femtosecond laser imaging system for the measurements of two-photon absorption (TPA), PL and the absolute TPE cross section.**<sup>7-17</sup> The home-made femtosecond Ti : sapphire laser optical system (repetition rate of 80 MHz) (Tsunami, Spectra-Physics, Santa Clara, CA, USA) was used in this study. **TPA measurement.** A femtosecond laser with a wavelength range of 720–820 nm and was used to excite TPA signals. A time-average luminescence photon count ( $F$ ) is proportional to the cross section ( $\delta$ ) of TPA and can be given as

$$F \sim \frac{1}{2} \delta \eta_2 \phi C \frac{g_p}{f\tau} \frac{8nP^2}{\pi\lambda} \quad (2)$$

, where  $C$  the concentration of the photoinitiator,  $\eta_2$  is the quantum efficiency of PL,  $\phi$  the luminescence collection efficiency of the system,  $P$  the average incident power,  $g_p$  the dimensionless quantity for degree of the second-order temporal coherence,  $f$  the pulse repetition rate,  $n$  the refractive index of the measurement medium,  $\lambda$  the excitation wavelength and  $\tau$  the excitation pulse width by full-width at half maximum. After the SF-10 prism pair compensation, the parameters which are the collection system, the pulse repetition rate, the concentration of the materials and the excitation power can be maintained the same at different excitation wavelengths with their corresponding excitation pulse widths. On the basis of the measured excitation pulse width, the measured fluorescence photon count and the excitation wavelength, the TPA was derived as  $\delta \times \eta_2$ . Via the SPC module, the photomultiplier

tubes (PMTs) (Hamamatsu, Japan) were used to collect the photoluminescence photon counts. The TPA can be given as

$$\delta\eta_2 \propto \lambda\tau F \quad (3)$$

An in-lab constructed autocorrelator was used to monitor the pulse widths of the different wavelengths after the objective. With 2 m ms<sup>-1</sup> speed of the galvanometer scanner, the excitation spectrum was measured 720-820 nm in wavelength with 3.0 mW excitation power. For all of GQD and GQD@polymers nanomaterials, **Fig. 3a-b** show the relative TPA spectrum as function of excitation wavelength.

**Measurement of the TPE absolute cross section.**<sup>7-17</sup> The TPE absolute cross section was measured the luminescence signal *via* femtosecond laser optical system mentioned above. The back aperture of the 20× objective lens (*NA* 0.256) was overfilled by expansion of the laser beams. For the multiphoton excitation, the diffraction-limited illumination of the sample was approximately achieved and analyzed. Under two-photon excitation and for the thick sample limit, the relation between time-averaged luminescence photon flux  $\langle F^{(n)}(t) \rangle$  and the incident power  $P(t)$  can be obtained. The formula can be given as

$$\langle F^{(n)}(t) \rangle = \frac{1}{n} \frac{g_p^{(n)}}{(f\tau)^{n-1}} \phi \eta \sigma_n C n_0 \frac{a_n (\text{NA})^{2n-4} \langle P(t) \rangle^n}{8\pi^{3-n} \lambda^{2n-3}} \quad (4)$$

, where  $C$  is the concentration of the fluorophore,  $n$  is the number of photons absorbed ( $n = 2$  for the TPE),  $\phi$  is the system collection efficiency,  $\tau$  is the laser pulse width,  $f$  is the laser repetition rate,  $\eta$  is the luminescence quantum efficiency (or QY) (one or TPE yields the same QY),<sup>7</sup> and  $\lambda$  is the excitation wavelength in vacuum,  $\sigma_n$  is the  $n$ -photon absorption cross section, and  $a_2 = 64$  for TPE.  $g_p^{(n)}$  is the  $n^{\text{th}}$ -order temporal coherence of the excitation source. Due to the limitation of resource we currently have,  $\langle F^{(n)}(t) \rangle$  is temporarily not able to be calculated and the values could be replaced by the integrated luminescence intensity with the symbol "Counts". As a result, the equation for action cross section ( $\eta\sigma_2$ ) is turned into

$$\eta\sigma_2 = \frac{\text{counts}}{\frac{1}{2} \frac{g_p^{(2)}}{f\tau} n_0 \phi C \frac{8\langle P(t) \rangle^2}{\pi\lambda}} \quad (5)$$

If it was with the same 2<sup>nd</sup>-order temporal coherence of the excitation source, the laser pulse width, laser repetition rate, incident power, system collection efficiency, wavelength and working concentration, the action cross section of TPE ( $\eta\sigma_2$ ) for a fluorophore as the reference compound is determined relative to the known action cross section, then the formula (5) is simplified as

$$(\eta\sigma_2)_2 = \frac{\text{counts}_2}{\text{counts}_1}(\eta\sigma_2)_1 \quad (6)$$

, where Sample 1 means the reference compound, and sample 2 means the fluorophore.

For careful concern, the known action cross section of TPE for fluorescein (Sigma-Aldrich Co., USA) and rhodamine B (Sigma-Aldrich Co., USA) was firstly used as the standard reference and fluorophore to calculate each other's action cross section and *vice versa*. At 800 nm in wavelength of femtosecond laser exposure, according to the previous studies, the action cross section of TPE for fluorescein and rhodamine B is 36.4 and 153.0 GM (1 GM = 10<sup>-50</sup> cm<sup>4</sup>s photon<sup>-1</sup>), respectively. The integrated TPL intensity for "Counts" was based on the spectra (**Fig. S11†**). TPL of fluorescein and rhodamine B was needed to be verified. By measuring the dependence of the emission intensity on the excitation power range of 20-80 mW, the results were shown in **Fig. S12†**. The dependence was observed to be quadratic, with exponents of 2.00 to 2.01 measured for increasing excitation power to determine the luminescence from TPE. Based on formula (6), the TPE action cross section of fluorescein and rhodamine B could be calculated as 34.7 and 151.2 GM (**Table S3†**). Compared to the data in the previous studies, there is less than 5 % in error that is the acceptable deviation. In other words, the action cross section of TPE for sample was available *via* formula (5) and (6). Further, select fluorescein (QY=0.72, dissolved in ddH<sub>2</sub>O, pH 11) as a standard references and the QYs of samples in **Table 2**, the absolute cross sections of TPE for GQD and GQD@polymers nanomaterials can be obtained, respectively, and showed in **Table 2**.

**Measurement of TPL spectrum.**<sup>2,8,9,16</sup> All of GQD and GQD@polymers nanomaterials were illuminated with the femtosecond laser system in an excitation wavelength of 800 nm (5.0 mW). Scanning area 200 μm × 200 μm, frequency: 10 kHz, 128 × 128 pixels/scan, pixel area= 1562.5 × 1562.5 nm<sup>2</sup> and a duration of 1.638 s exposure time/scan= 100 μs per pixel per scan. For 800 nm-excitation:  $t = 4.53$  ms × number of scans and obtain the data. The signal collection was used by a 40× oil-immersion objective (*NA* 1.3) and the detected wavelength (300-650 nm) was by the spectrum photometer.

**Femtosecond laser imaging system (for fluorescence lifetime imaging microscopy).** The femtosecond laser imaging system is coupled with the fluorescence (or luminescence) lifetime imaging microscopy (FLIM) system based on a time-correlated single photon counting (TCSPC) module (PicoHarp 300, PicoQuant). Main components of this instrument/microscope comprise a femtosecond, titanium-sapphire (ti-sa) laser (Tsunami, Spectra-Physics, USA) with a pulse width of less than 100 fs and a repetition rate of 80 MHz, an inverted optical microscope (Axiovert 200, Zeiss, Germany), a triple-axis sample-positioning stage (ProScan<sup>TM</sup>II, Prior, UK), an acousto-optic modulator (AOM) (23080-x-1.06-LTD, Neos, USA), PMTs (H5783P, Hamamatsu, Japan), a data acquisition (DAQ) card with a field-programmable gate array (FPGA) module (PCI-7831R, National Instruments, USA), a x-y galvanometer scanner (6215H, Cambridge, USA) and a z-axis piezoelectric nano-positioning stage (Nano-F100, Mad City Labs, USA). A detailed description of the multiphoton fabrication instrument can be found in the previous studies.<sup>8,9</sup> For FLIM, the TCSPC module is integrated into the main control platform based on LabVIEW programming, which triggers the synchronic signal via the FPGA module, collects the luminescence time-to-digital data via a USB 2.0 interface, and then constructs the luminescence lifetime image under LabVIEW. The time-to-digital data from different pixels is separated by inserting a marker signal from scanning synchronic trigger. To facilitate three-dimensional data analysis and lifetime image, the LabVIEW program also records the scanning parameters corresponding to the time-to-digital data. The timer overflow signal of the TCSPC is removed, allowing the accumulated time-to-digital data of each pixel to form a histogram. Nonlinear least square algorithm is used to fit the luminescence lifetime decay curve for each pixel. The FLIM image can be displayed with a resolution of 0.1 ns under the main control platform according to the fitting lifetime data of each pixel and the pixel scanning information.

**Calculation of radiative and non-radiative decay rates.**<sup>7,16</sup> When investigating the emission characteristics of fluorescent dyes in diverse environments, PL QY and lifetime are both major parameters. The QY (Q) can be given as

$$Q = \frac{\Gamma}{\Gamma + k} \quad (7)$$

, where  $k$  is the non-radiative decay rate and  $\Gamma$  is the radiative decay rate.

One or TPE yields the same quantum yield.<sup>7</sup> Lifetime is usually defined as the average time required for an electron in the excited state to decay to the ground state. The fluorescence (or luminescence) lifetime  $\tau$  can be also relative to the decay rates and expressed as

$$\tau = \frac{1}{\Gamma + k} \quad (8)$$

Following Eq.(7) and (8), the radiative and non-radiative decay rates can be calculated.

**Cytotoxicity assay. For 1 day incubation.**  $5 \times 10^3$  A549 cells were cultured and incubated in an incubator (37°C with 5% CO<sub>2</sub> in air) in the dark overnight. All of GQD- and GQD@polymers-nanomaterials (delivered dose: 10-100  $\mu\text{g mL}^{-1}$ ) were respectively added to the incubated cells and incubated in an incubator (37°C with 5% CO<sub>2</sub> in air) in the dark overnight. Wash out the nonspecific binding with the new culture medium and repeat for several times. After the trypsinization of cells, centrifugation in 1200 rpm for 10 min was to collect the pellets. Then, follow the previous studies<sup>18,19</sup> to conduct the Methyl thiazolyl tetrazolium (MTT) assay (Sigma-Aldrich Co., USA) with an ELISA reader (Thermo Electron, USA). **For 4 day incubation.**  $5 \times 10^3$  A549 cells were cultured and incubated in an incubator (37°C with 5% CO<sub>2</sub> in air) in the dark overnight. All of GQD- and GQD@polymers-nanomaterials (delivered dose: 50  $\mu\text{g mL}^{-1}$ ) were added to the incubated cells and incubated in an incubator (37°C with 5% CO<sub>2</sub> in air) in the dark for 4 days, respectively. Wash out the nonspecific binding with the new culture medium and repeat for several times. After the trypsinization of cells, centrifugation in 1200 rpm for 10 min was to collect the pellets. Then, follow the previous studies<sup>18,19</sup> to conduct the MTT assay (Sigma-Aldrich Co., USA) with an ELISA reader (Thermo Electron, USA). Data were shown as the means  $\pm$  SD (n = 6).

**Reactive Oxygen Species (ROS) detection. For 1 day incubation.** *Superoxide radical anion* ( $\text{O}_2^{\cdot-}$ ). GQD- and GQD@polymers-nanomaterials were delivered in the concentration from 10 to 100  $\mu\text{g mL}^{-1}$ . Nanomaterial-treated-A549 cells ( $5 \times 10^3$  cells) were respectively incubated overnight at 37 °C, and mixed, incubated with 2,3-bis(2-methoxy-4-nitro-5-sulfohenyl)-2H-tetrazolium-5-carboxanilide (XTT) (0.45 mM) (Sigma-Aldrich Co., USA) for 5 h in the dark.<sup>20</sup> XTT would interact with  $\text{O}_2^{\cdot-}$  and produce the XTT-formazan generating strong absorption (470 nm in wavelength), which was monitored with UV-vis spectrometer (U-4100, Hitachi, Japan). Data were shown as the means  $\pm$  SD (n = 6). *Singlet oxygen* ( $^1\text{O}_2$ ). GQD- and GQD@polymers-nanomaterials were delivered in the concentration from 10 to 100  $\mu\text{g mL}^{-1}$ . Nnomaterial-treated-A549 cells ( $5 \times 10^3$ ) were respectively incubated overnight at 37 °C, and then 1  $\mu\text{M}$  of Singlet Oxygen Sensor Green (SOSG) Reagent (Ex/Em: 488/525 nm) (Invitrogen, USA) was added. Signals were collected by a fluorescence spectrophotometer (F-7000, Hitachi, Japan) following the instructions.<sup>2,4</sup> Data were shown as the means  $\pm$  SD (n = 6). *Glutathione*

( $\gamma$ -L-glutamyl-L-cysteinyl-glycine, GSH) oxidation ( $O_2^{\cdot-}$ ) (the Ellman's assay). GQD- and GQD@polymers-nanomaterials were delivered in the concentration from 10 to 100  $\mu\text{g mL}^{-1}$ . Nanomaterial-treated-A549 cells ( $5 \times 10^3$  cells) were respectively incubated overnight at 37 °C, and mixed, incubated with 50 mM bicarbonate buffer (pH 8.6) and GSH/0.8mM bicarbonate buffer in dark. Then, incubate in an incubator for 2 h at 37 °C. After this, the following experiments were according to the previous studies.<sup>21-23</sup> Loss of GSH (%) = (absorbance difference between of sample and negative control / absorbance of negative control)  $\times$  100 %. Data were shown as the means  $\pm$  SD (n = 6). **For 4 day incubation.** Superoxide radical anion ( $O_2^{\cdot-}$ ). GQD- and GQD@polymers-nanomaterials were delivered in a concentration of 50  $\mu\text{g mL}^{-1}$ . Nanomaterial-treated-A549 cells ( $5 \times 10^3$  cells) were respectively incubated for 4 day at 37 °C, and mixed, incubated with XTT (0.45 mM) (Sigma-Aldrich Co., USA) for 5 h in the dark.<sup>20</sup> XTT would interact with  $O_2^{\cdot-}$  and produce the XTT-formazan generating strong absorption (470 nm in wavelength), which was monitored with UV-vis spectrometer (U-4100, Hitachi, Japan). Data were shown as the means  $\pm$  SD (n = 6). Singlet oxygen ( $^1O_2$ ). GQD- and GQD@polymers-nanomaterials were delivered in a concentration of 50  $\mu\text{g mL}^{-1}$ . Nanomaterial-treated-A549 cells ( $5 \times 10^3$ ) were respectively incubated for 4 day at 37 °C, and then 1  $\mu\text{M}$  of SOSG Reagent (Ex/Em: 488/525 nm) (Invitrogen, USA) was added. Signals were collected by a fluorescence spectrophotometer (F-7000, Hitachi, Japan) following the instructions.<sup>2,4</sup> Data were shown as the means  $\pm$  SD (n = 6). GSH oxidation ( $O_2^{\cdot-}$ ) (the Ellman's assay). GQD- and GQD@polymers-nanomaterials were delivered in a concentration of 50  $\mu\text{g mL}^{-1}$ . Nanomaterial-treated-A549 cells ( $5 \times 10^3$  cells) were respectively incubated for 4 day at 37 °C, and mixed, incubated with 50 mM bicarbonate buffer (pH 8.6) and GSH/0.8mM bicarbonate buffer in dark. Then, incubate in an incubator for 2 h at 37 °C. After this, the following experiments were according to the previous studies.<sup>21-23</sup> Loss of GSH (%) = (absorbance difference between of sample and negative control / absorbance of negative control)  $\times$  100 %. Data were shown as the means  $\pm$  SD (n = 6).

### **Antibody conjugation**

The absorbance of a quantity of antibody (epidermal growth factor receptor antibody (Ab<sub>EGFR</sub>) (Antagene, USA)) was recorded by UV-vis spectroscopy (Abs: approximately 276 nm). By the electrostatic interaction, the nanomaterials were mixed with the same quantity antibody for 30 min of incubation at 4 °C in the dark and centrifuge (83000 rpm) to remove excess antibody, and then the nanomaterial-Ab<sub>EGFR</sub> was prepared. On the other hand, keep the supernatant and measure its absorbance. The difference in absorbance between the collected supernatant and the original antibody was estimated. Consequentially, the quantity of

the antibody conjugated on the nanomaterials was calculated by Lambert-Beer's law. There was approximately 0.095  $\mu\text{g}$  of  $\text{Ab}_{\text{EGFR}}$  conjugated on 1  $\mu\text{g}$  of nanomaterial, which meant the efficiency of conjugation was approximately 9.5%.

#### **Cell culture of human squamous carcinoma cell line (A431 cells)**

A431 cells were cultured in EMEM (EBSS) + 2mM Glutamine + 1% Non Essential Amino Acids + 10% Foetal Bovine Serum at 37°C under 5%  $\text{CO}_2$  in air. The cells were collected by trypsinization and placed onto a 10 cm tissue culture Petri dish, then allowed to grow for 2 - 4 days.

#### **TPL image**

$5 \times 10^3$  human squamous carcinoma cell line A431 cells per well in a 96-well culture plate were for overnight of incubation in the dark at 37°C with 5%  $\text{CO}_2$  in air. All of the  $\text{GQD@POAA@PSS-Ab}_{\text{EGFR}}$  (delivered dose of material: 50  $\mu\text{g mL}^{-1}$ .) were respectively added to the incubated cells to process the interaction of antibody-antigen for 2.5 h of incubation in the dark at 37°C. Remove and replace with the new culture medium and repeat for 3 to 5 times to wash out the nonspecific binding. The cells were embedded in a collagen matrix to mimic the three-dimensional epithelium tissue. And the TPL images of  $\text{GQD@POAA@PSS-Ab}_{\text{EGFR}}$ -treated-A431 cells were observed using a nonlinear femtosecond laser microscopy optical system under TPE.

FTIR was used to analyze the exposed functional groups of the GQDs (**Fig. S1†**). Results showed characteristic bands of GQDs for epoxy stretching about  $951\text{ cm}^{-1}$ , C–O stretching about  $1104\text{ cm}^{-1}$ , tertiary alcoholic C–OH bending about  $1312\text{ cm}^{-1}$ , symmetric carboxylate  $\text{C}(\text{=O})_2^-$  stretching about  $1390\text{ cm}^{-1}$ , asymmetric carboxylate  $\text{C}(\text{=O})_2^-$  stretching about  $1566\text{ cm}^{-1}$ , C=C ring stretching about  $1652\text{ cm}^{-1}$ , broad O–H stretching about  $2293$  and  $2412\text{ cm}^{-1}$ , and cyclic alkanes, C–H stretching, intermolecular hydrogen bonded and O–H stretching about  $3367\text{ cm}^{-1}$ .

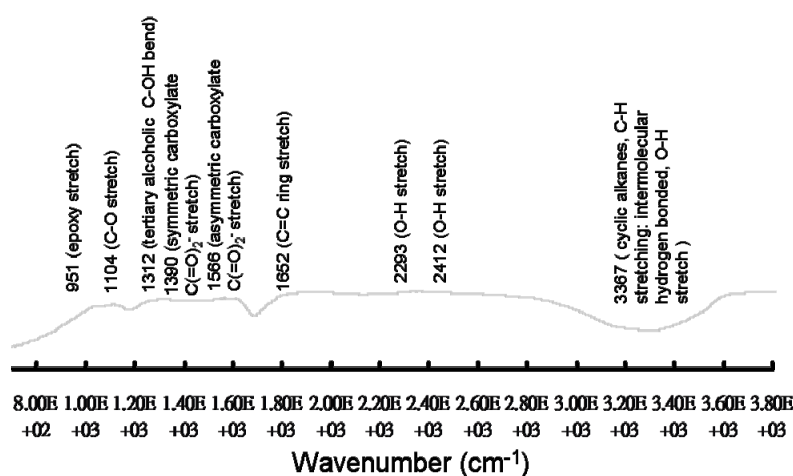


**Fig. S1** FTIR spectrum of GQDs.

AFM image of a  $0.82\text{ nm}$  thick single layer of GQDs (**Fig. 1c**), which was dried on a mica surface. Single-layer GQD@PAH and GQD@PAH@PAA were  $0.93$  and  $1.12\text{ nm}$  thick, respectively (**Fig. S2a–b†**). Single-layer GQD@POAA, GQD@POAA@PAA, and GQD@POAA@PSS were approximately  $0.91$ ,  $1.31$ , and  $1.42\text{ nm}$  thick, respectively (**Fig. S2c–e†**). PAH, PAA, POAA, and PSS were successfully adsorbed on the surfaces of the GQD through electrostatic interaction.

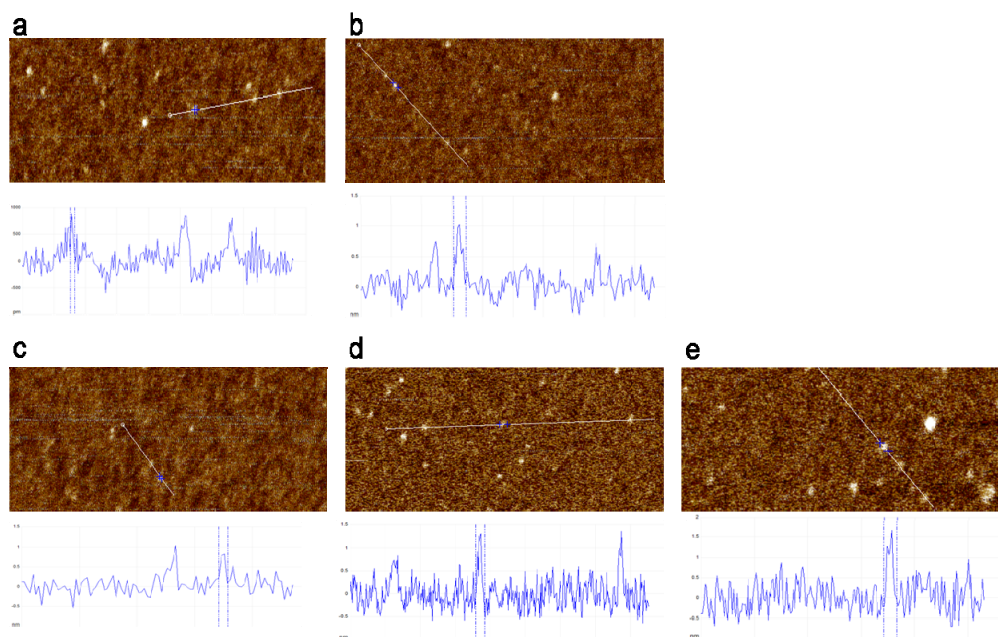


**Fig. S2** AFM images of (a) GQD@PAH, (b) GQD@PAH@PAA, (c) GQD@POAA, (d) GQD@POAA@PAA, and (e) GQD@POAA@PSS on mica. The height difference between two arrows (the GQD-based nanomaterial and mica) is approximately 0.9–1.4 nm, consistent with the thickness of a single layer of the GQD@polymers nanomaterials.

**Fig. S3c†** shows the following: the characteristic bands of GQD@PAH at approximately  $1104\text{-cm}^{-1}$  for C–O stretching,  $1663\text{ cm}^{-1}$  for ring C=C stretching,  $2381\text{ cm}^{-1}$  for broad N–H stretching, and  $3354\text{ cm}^{-1}$  for C–H stretching; the characteristic bands of GQD@PAH@PAA at approximately  $1133\text{ cm}^{-1}$  for C–O stretching,  $1392\text{ cm}^{-1}$  for symmetric carboxylate  $\text{C}(=\text{O})_2^-$  stretching,  $1663\text{ cm}^{-1}$  for ring C=C stretching,  $2356$  and  $2382\text{ cm}^{-1}$  for broad O–H stretching,  $3361\text{ cm}^{-1}$  for C–H stretching, intermolecular hydrogen bonded and O–H stretching (**Fig. S3b†**); the characteristic bands of GQD@POAA at approximately  $1108\text{ cm}^{-1}$  for C–O stretching,  $1302\text{ cm}^{-1}$  for tertiary alcoholic C–OH bending,  $1654\text{ cm}^{-1}$  for ring C=C stretching,  $2302$  and  $2400\text{ cm}^{-1}$  for broad N–H stretching, and  $3356\text{ cm}^{-1}$  for C–H stretching (**Fig. S3c†**); the characteristic bands of GQD@POAA@PAA at approximately  $1127\text{ cm}^{-1}$  for C–O stretching,  $1392\text{ cm}^{-1}$  for symmetric carboxylate  $\text{C}(=\text{O})_2^-$  stretching,  $1664\text{ cm}^{-1}$  for ring C=C stretching,  $2351$  and  $2382\text{ cm}^{-1}$  for broad O–H stretching,  $3366\text{ cm}^{-1}$  for C–H stretching (intermolecular hydrogen bonded), and O–H stretching (**Fig. S3d†**); the characteristic bands of GQD@POAA@PSS at approximately  $1132\text{ cm}^{-1}$  for C–O stretching,  $1661\text{ cm}^{-1}$  for ring C=C stretching, and  $3366\text{ cm}^{-1}$  for primary sulphonamide (**Fig. S3e†**).

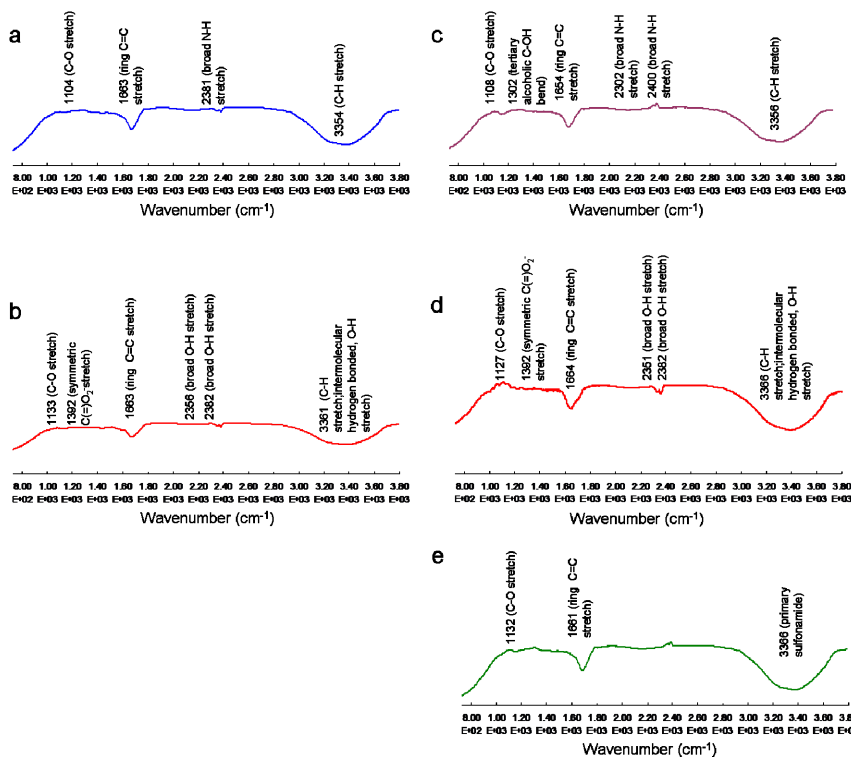


**Fig. S3** FTIR spectra of (a) GQD@PAH, (b) GQD@PAH@PAA, (c) GQD@POAA, (d) GQD@POAA@PAA, and (e) GQD@POAA@PSS.

Control experiment results. **Fig. S4a†** shows the characteristic bands of GQDs at approximately  $951\text{ cm}^{-1}$  for epoxy stretching,  $1104\text{ cm}^{-1}$  for C–O stretching,  $1302\text{ cm}^{-1}$  for tertiary alcoholic C–OH bending,  $1390\text{ cm}^{-1}$  for symmetric carboxylate  $\text{C}(=\text{O})_2^-$  stretching,  $1566\text{ cm}^{-1}$  for asymmetric carboxylate  $\text{C}(=\text{O})_2^-$  stretching,  $1652\text{ cm}^{-1}$  for C=C ring stretching,  $2293$  and  $2412\text{ cm}^{-1}$  for broad O–H stretching,  $3367\text{ cm}^{-1}$  for cyclic alkanes, C–H stretching, intermolecular hydrogen bonded and O–H stretching. Also shown are the characteristic bands of PAH at approximately  $1022$  and  $1190\text{ cm}^{-1}$  for C–N stretching,  $1261\text{ cm}^{-1}$  for C–H bending,  $1456\text{ cm}^{-1}$  for N–H and C–H bending,  $1540$  and  $1652\text{ cm}^{-1}$  for N–H bending and scissor,  $2293\text{ cm}^{-1}$  for broad N–H stretching, and  $3392\text{ cm}^{-1}$  for primary amine salt stretching (**Fig. S4b†**); the characteristic bands of PAA at approximately  $1202$  and  $1300\text{ cm}^{-1}$  for C–O stretching,  $1463\text{ cm}^{-1}$  for symmetric carboxylate  $\text{C}(=\text{O})_2^-$  stretching,  $1668$  and  $1724\text{ cm}^{-1}$  for asymmetric  $\text{C}(=\text{O})_2^-$  stretching,  $3391\text{ cm}^{-1}$  for broad dimer carboxylic acid stretching (**Fig. S4c†**); the characteristic bands of POAA and the characteristic bands of chitosan at approximately  $964$ ,  $1110$ , and  $1154\text{ cm}^{-1}$  for C–O stretching,  $1252$ ,  $1294$ ,  $1352$ , and  $1476\text{ cm}^{-1}$  for C–H stretching,  $2892\text{ cm}^{-1}$  for C–H stretching, and  $3381\text{ cm}^{-1}$  for primary amine stretching (**Fig. S4d†**); the characteristic bands of PSS at approximately  $779$  and  $841\text{ cm}^{-1}$  for aromatic C–H bending,  $1013$  and  $1040\text{ cm}^{-1}$  for

in-plane C–H bending, 1132, 1186, 1422 and 1510  $\text{cm}^{-1}$  for C–H bending, 1662  $\text{cm}^{-1}$  for ring C=C stretching, 2946  $\text{cm}^{-1}$  for broad C–H stretching, and 3467  $\text{cm}^{-1}$  for primary sulphonamide (**Fig. S4e†**).

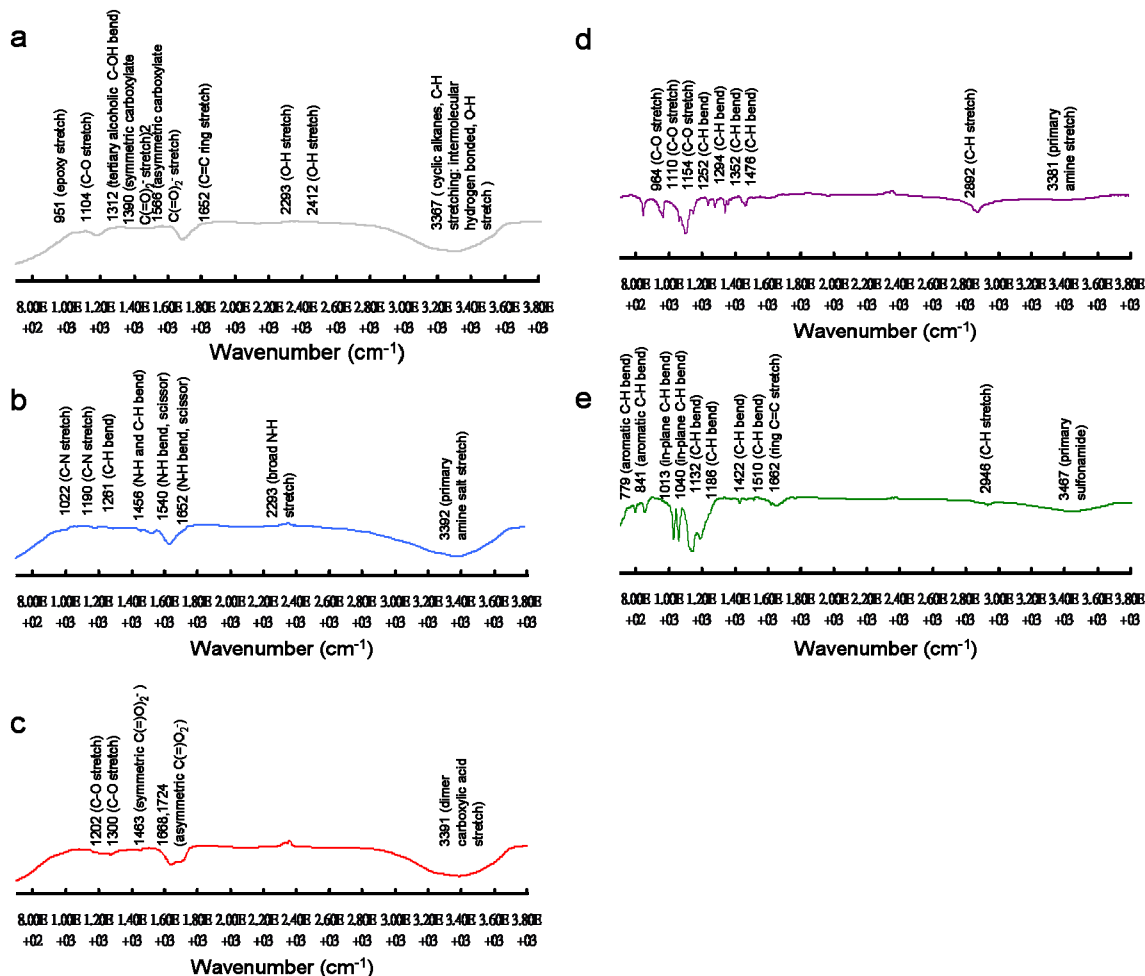


**Fig. S4** FTIR spectra of (a) GQDs, (b) PAH, (c) PAA, (d) POAA, and (e) PSS.

UV-vis spectrometer was used to confirm whether GQD-based nanomaterials were successfully synthesised and prepared. The GQDs show peaks at approximately 219 nm ( $\pi$ - $\pi^*$  transition of aromatic C=C bonds) and 320 nm ( $n$ - $\pi^*$  transition of the C=O shoulder). GQD@PAH exhibits absorptions at approximately 222 and 321 nm; the characteristic peaks of GQD@PAH@PAA exhibit a red shift of approximately 228 and 323 nm (**Fig. S5a† and S5c†**). The characteristic peaks of GQD@POAA exhibit red-shifted absorption peaks at approximately 224 and 323 nm; GQD@POAA@PAA shows the absorption peaks at approximately 217 and 324 nm; GQD@POAA@PSS shows red-shifted absorption at approximately 225, and 324 nm, and peaked around 263 nm due to the coating of PSS (**Fig. S5b-c†**).

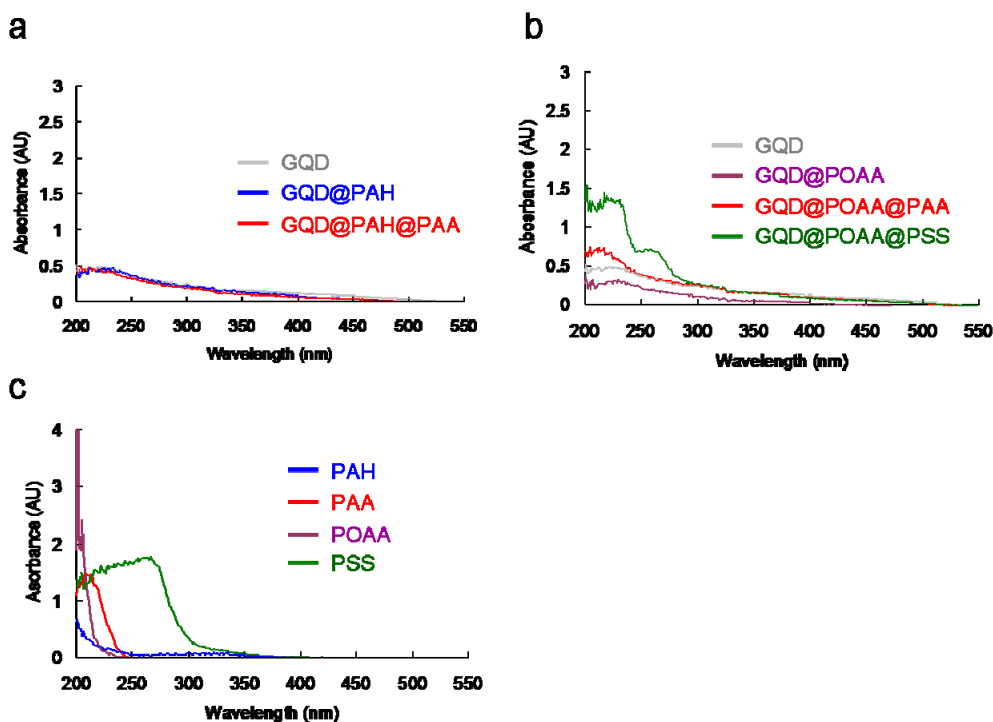


**Fig. S5** UV-vis spectra of (a) GQDs, GQD@PAH, GQD@PAH@PAA, (b) GQDs, GQD@POAA, GQD@POAA@PAA, GQD@POAA@PSS, and (c) polymers.

Raman spectroscopy to examine the crystallinity of graphite, graphene, graphene oxide, GQD and GQD-based materials (**Fig. S6†**). The major feature bands of graphite are the so-called G band ( $\sim 1605\text{ cm}^{-1}$ ), which comes from in-plane vibration of  $\text{sp}^2$  hybridized C-C bonds in a two dimensional hexagonal lattice; the D band that corresponds to the defect, disorder, and  $\text{sp}^3$ -hybridized carbon in graphene layers by breaking the translational symmetry of the lattice occurred at about  $1380\text{ cm}^{-1}$  (**Fig. S6a†**). It can be seen that the integrated intensity ratio of the D and G bands ( $I_D/I_G$  ratio), which represent the degree of disorder, was 0.106. Besides, the D and G bands of graphene (**Fig. S6b†**) and graphene oxide (**Fig. S6c†**) and are  $1382$ ,  $1609$ ,  $1383$  and  $1601\text{ cm}^{-1}$ , respectively. Then, the  $I_D/I_G$  ratio of graphene and graphene oxide is 1.11 and 1.03, respectively. For GQD, the major feature bands are the so-called D ( $\sim 1384\text{ cm}^{-1}$ ) and the G band ( $\sim 1603\text{ cm}^{-1}$ ); the  $I_D/I_G$  ratio is 0.82, indicating the successful conversion from graphite, graphene oxide to GQD (**Fig. S6d†**). After the conjugation of PAH and PAA, in sequence, the position of the D band and G band shift from  $1384$  to  $1354\text{ cm}^{-1}$  and from  $1603\text{ cm}^{-1}$  to  $1586\text{ cm}^{-1}$ , respectively (**Fig. S6d†**). After the conjugation of POAA and PAA, in sequence, the position of the D band and G band shift from  $1384$  to  $1356\text{ cm}^{-1}$  and from  $1603$  to  $1589\text{ cm}^{-1}$ , respectively; the same results were obtained for the conjugation of POAA and PSS (D:  $\sim 1357\text{ cm}^{-1}$ , G:  $\sim 1590\text{ cm}^{-1}$ ) in sequence (**Fig. S6e†**). The  $I_D/I_G$  intensity ratios of

GQDs, GQD@PAH, GQD@PAH@PAA, GQD@POAA, GQD@POAA@PAA, and GQD@POAA@PSS were 0.82, 0.82, 0.83, 0.82, 0.83, and 0.83, respectively, probably because PAH, PAA, POAA, PAA, and PSS, are electron-donor molecules that cause high-frequency, tangential, vibrational modes of the carbon molecules in the GQD-based nanomaterials to shift to lower frequencies.<sup>24</sup>

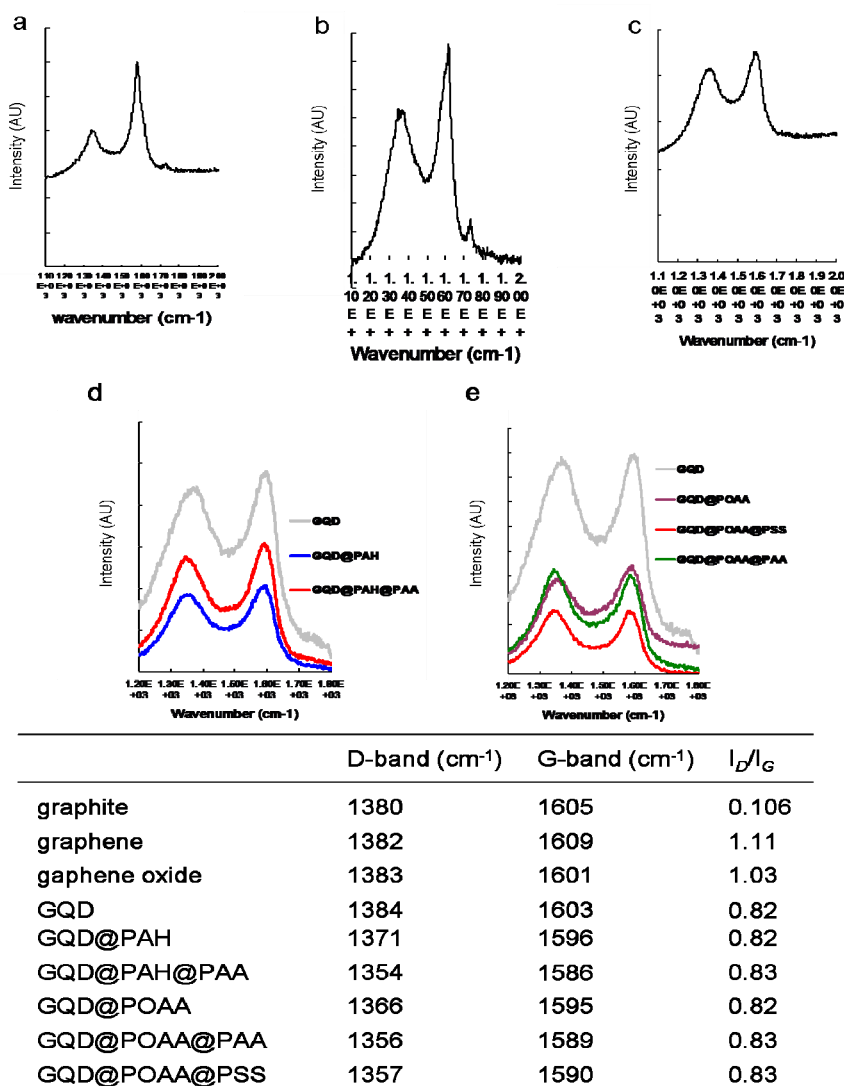


**Fig. S6** Raman spectra of (a) graphite, (b) graphene, (c) graphene oxide, (d) GQDs, GQD@PAH, GQD@PAH@PAA, (e) GQDs, GQD@POAA, GQD@POAA@PAA, and GQD@POAA@PSS. The data was summarized in the Table.

The surface chemistry of graphene oxide, which predominant contain carbon atoms was examined by XPS. The deconvoluted C(1s) spectra of graphene oxide showed a nonoxygenated ring (C–C/C=C, 285.3 eV), C–O bonds (286.4 eV), and

carbonyl (C=O, 287.9 eV) and carboxylate groups (O=C–O, 289.4 eV) for graphene oxide (Fig. S7†).

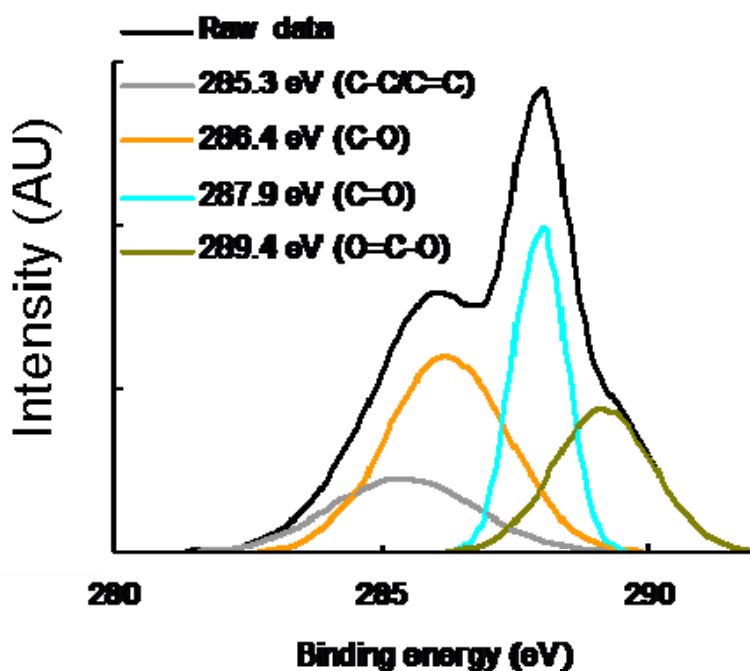


**Fig. S7** The surface chemistry change of graphene oxide was determined by XPS. The deconvoluted C(1s) XPS spectra and fitted peaks (using Gaussian function): C–C/C=C, C–O, C=O, and O–C–O for graphene oxide.

**Fig. S8†** shows the PL spectra of GQD-based nanomaterials excited from 390 nm to 480 nm by a fluorescence spectrometer. For GQDs, an emitted peak is observed at approximately 489 nm, and it shifts to approximately 526 nm with an increase in the excitation wavelength. The PL intensity decreases and shows a red-shifted PL peak (**Fig. S8a†**). PL spectra of GQD@polymers exhibit a similar trend for the same treatment (**Fig. S8b-f†**). The results of FTIR and XPS showed that the functional groups on the surface of the GQDs form a surface state energy level between the  $\pi$  and the  $\pi^*$  states of the C=C  $sp^2$  clusters; the energy level is influenced by the band gap of the  $\sigma$  and  $\sigma^*$  states of the  $sp^3$  matrix and is strongly confined.<sup>25</sup> Because of the difference in chemical bonding between the C=C and C=O groups, the variation of the  $\pi^*$  energy states is expected. Thus, a distribution  $\pi^*$  band (C=C and C=O) results. Radiative recombination of electron–hole pairs in such  $sp^2$  clusters can generate fluorescence.<sup>26</sup> Further, the excitation wavelength dependence of the emission wavelength and intensity is commonly observed in carbon-based QDs,<sup>27,28</sup> and it has been suggested that emissive traps, electronic conjugated structure, and free zigzag

sites are the main causes for the dependence.<sup>29,30</sup> When the GQD-based nanomaterials are exposed to a laser beam with an excitation wavelength, a surface state emissive trap dominates the emission. With a change in the excitation wavelength, another corresponding surface state emissive trap becomes dominant. Consequently, the emissive traps induced by surface states of the functional groups should play a crucial role in the emission of GQD-based nanomaterials. This explains the excitation wavelength dependence of GQD-based nanomaterials.<sup>31</sup>

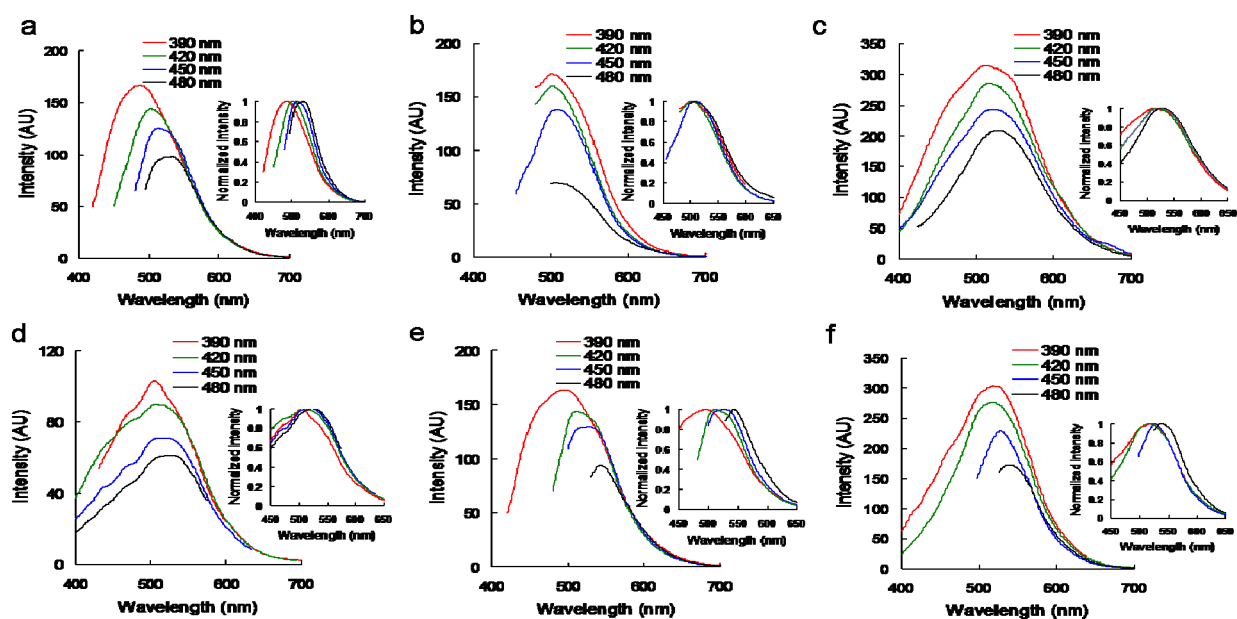


**Fig. S8** PL spectra of the (a) GQDs, (b) GQD@PAH, (c) GQD@PAH@PAA, (d) GQD@POAA, (e) GQD@POAA@PAA, and (f) GQD@POAA@PSS (inset: with the intensity normalised). The excitation wavelength was in the range 390–480 nm.

Results (**Fig. S1-S8†**) of these characterizations confirmed the polymers was passivated on the surface of the GQDs nanomaterials.

GQD and GQD@polymers displayed high biocompatibility by MTT assay (**Fig. S9a†**), as well as ROS assays (**Fig. S9b-d†**) These determinations showed that the GQD and GQD@polymers did not induce any oxidative stress at any concentration, reflecting high biocompatibility.

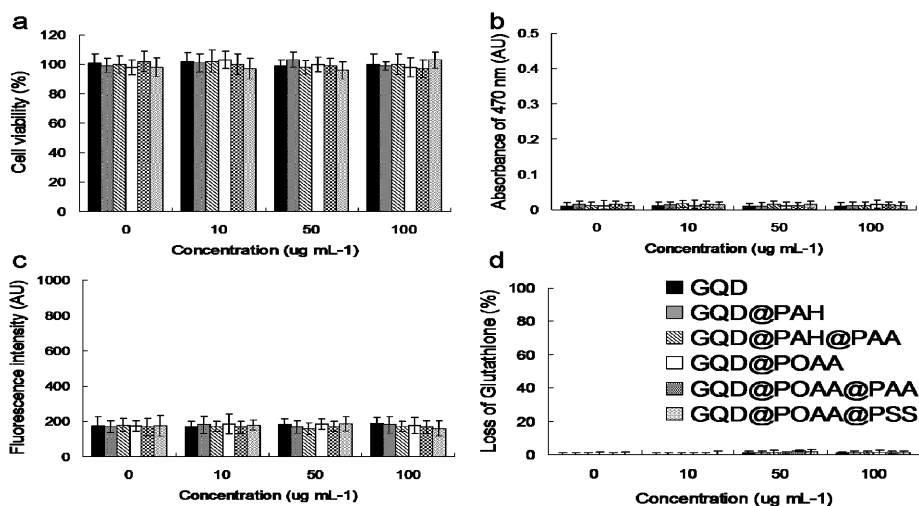


**Fig. S9** (a) Estimation of the viability of the GQD- and GQD@polymers-treated A549 cells. (b) After A549 cells were treated with GQD and GQD@polymers, superoxide radical anion ( $O_2^{\cdot-}$ ) was generated. XTT was used to monitor the generated  $O_2^{\cdot-}$  and record the absorbance at 470 nm. (c) SOSG Reagent was used to detect singlet oxygen ( $^1O_2$ ). Measurements of  $^1O_2$  were conducted by monitoring the GQD- and GQD@polymers-treated A549 cells. (d) GSH was used to monitor the oxidative stress of the GQD- and GQD@polymers-treated A549 cells (dose of GQD-based nanomaterials delivered: 0–100  $\mu\text{g mL}^{-1}$ ). Data shown are means  $\pm$  SD ( $n = 6$ ).

A431 skin cancer cells with the overexpression of EGFRs on the surface were selected as our experimental template. To increase specific and efficient targeting, the anti-EGFR antibody was coated with materials. To demonstrate the outstanding two-photon properties of GQD@POAA@PSS, generation of nonreactive oxygen species-dependent oxidative stress on the cells and effectiveness of the materials in serving as a two-photon contrast agent, **Fig. S10†** displays the TPL images of the material-Ab<sub>EGFR</sub>-treated A431 cells with different depths at a wavelength of 800 nm under TPE. To imitate the 3D epithelium tissue, the embedded cells in a collagen matrix were also used. At a depth of 85  $\mu\text{m}$ , the TPL was illuminated from (**Fig. S10a†**) GQD@POAA@PSS-Ab<sub>EGFR</sub>-treated cells. TPL imaging of the GQD@POAA@PSS-treated cells with no antibody conjugation demonstrated nearly no attachment on the cell surface and internalization into the cell (**Fig. S10b†**). The TPL signal corresponded to bright rings with a distribution throughout the cellular membrane, which is associated with a characteristic pattern of successful Ab<sub>EGFR</sub> labeling. In addition, two-photon autofluorescence (TPAF) image (**Fig. S10c†**) which was emitted from intrinsic fluorophores of the cancer cells can not be observed with 5 mW of TPE in unlabeled cells.



**Fig. S10** TPL images of (a) GQD@POAA@PSS-Ab<sub>EGFR</sub>-treated A431 cells and (b) GQD@POAA@PSS-treated A431 cells; (c) TPAF image of unlabeled cells at a depth of 85 μm with a TPE power of 5 mW. Excitation wavelength: 800 nm. Delivered dose of material: 50 μg mL<sup>-1</sup>.

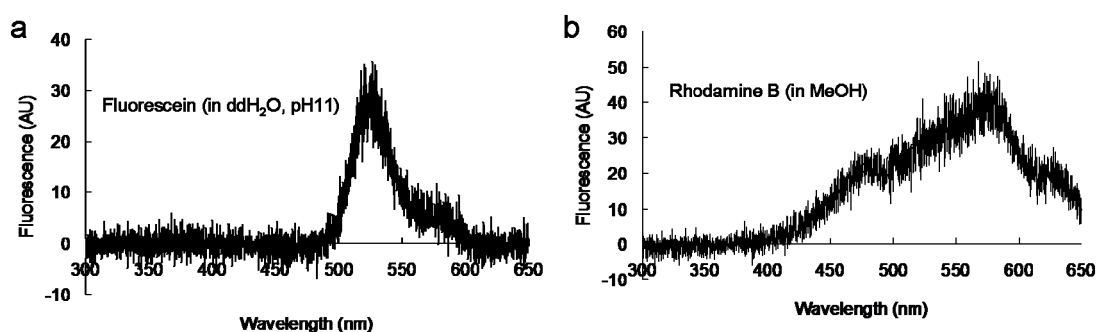


**Fig. S11** TPL spectra of (a) fluorescein (in ddH<sub>2</sub>O, pH 11) and (b) rhodamine B (in methanol) (Sigma Aldrich Co., USA). Both solutions were exposed to the femtosecond laser. The TPE wavelength was 800 nm.

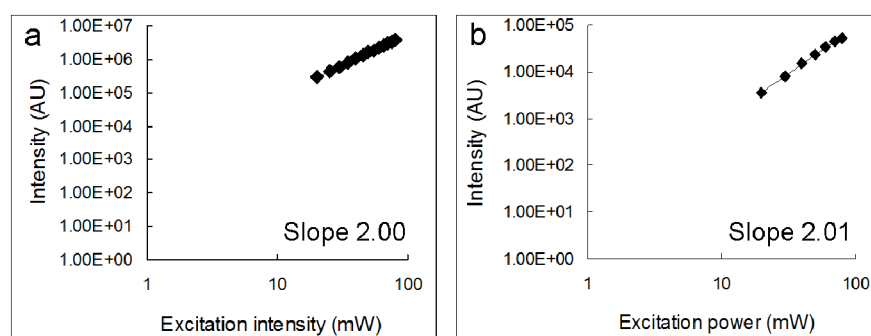


**Fig. S12** Plots of dependence of TPE luminescence on excitation intensity for (a) fluorescein (in ddH<sub>2</sub>O, pH 11) and (b) rhodamine B (in methanol). Both solutions were exposed to the femtosecond laser for the power range from 20 to 80 mW. The

TPE wavelength was 800 nm. The slope is indicated in each figure. Furthermore,  $R^2 > 0.99$ .

**Table. S1** O(1s)/C(1s) atomic ratio, carbon bonding composition determined by the XPS for GQDs.

Atomic ratio O(1s)/C(1s)	Carbon bonding composition (%)			
	C-C/C=C	C-O	C=O	O-C=O
24.2%	75	5	7	13

**Table. S2** Lifetime data and the parameter obtained by the exponential fitting while monitoring the emission at an excitation wavelength of 800 nm.

	3 exp fitting model: ( $a_0 \cdot \exp(a_1 x) + a_2 \cdot \exp(a_3 x) + a_4 \cdot \exp(a_5 x) - a_6$ )							lifetime 1	lifetime 2	lifetime 3	Ave lifetime (ns)
	a0	a1	a2	a3	a4	a5	a6				
GQD	1643.49	-2.142-8	5716.19	-0.78845	2637.85	-0.30877	487.9	0.466749	1.268318	3.238657	1.656422353
GQD@PAH	980.469	-9.7313	4165.7	-1.26382	1524.58	-0.27136	72.8813	0.102761	0.733235	3.6851-2	1.315217008
GQD@PAH@PAA	1099.85	-8.5967	5624.63	-1.4125	3582.81	-0.32075	174.963	0.116324	0.707965	3.117654	1.482440059
GQD@POAA	4074.78	-10.81-3	9105.01	-1.26644	3911.39	-0.32355	139.985	0.09247	0.789615	3.090674	1.150013049
GQD@POAA@PAA	2312	-5.86655	3277.22	-1.38493	1525.76	-0.27696	56.3208	0.170458	0.921718	3.610578	1.30191289
GQD@POAA@PSS	3624.9	-11.397	8563.59	-1.42952	4365.35	-0.3539	157.495	0.087742	0.699536	2.825681	1.12624496

**Table. S3** The action TPE cross sections of fluorescein (in ddH<sub>2</sub>O, pH 11) and rhodamine B (in methanol). The TPE wavelength is 800 nm.

Excitation wavelength at 800 nm action cross section, $\eta \sigma^2$ (GM, $10^{-50} \text{cm}^4 \text{s/photon}$ )	Fluorescein ( in ddH <sub>2</sub> O, pH 11)	Rhodamine B (in methanol)
	34.7	151.2

## Reference

- 1 W. S. Hummers and R. E. Offeman, *J. Am. Chem. Soc.*, 1958, **80**, 1339.
- 2 W. S. Kuo, Y. T. Chang, K. C. Cho, K. C. Chiu, C. H. Lien, C. S. Yeh and S. J. Chen, *Biomaterials*, 2012, **33**, 3270-3278.
- 3 W. S. Kuo, C. N. Chang, Y. T. Chang, M .H. Yang, Y. H. Chien, S. J. Chen and C. S. Yeh, *Angew. Chem. Int. Ed.*, 2010, **49**, 2711-2715.
- 4 W. S. Kuo, C. N. Chang, Y. T. Chang and C. S. Yeh, *Chem. Commun.*, 2009,

4853-4855.

- 5 R. Sjoback, J. Nygren and M. Kubista, *Spectrochimica. Acta A.*, 1995, **51**, L7-L21.
- 6 D. M. Togashi, B. Szczupak, A. G. Pyder, A. Calvet and M O'Loughlin, *J. Phys. Chem. A.*, 2009, **113**, 2757-2767.
- 7 C. Y. Lin, C. H. Clien, K. C. Cho, C. Y. Chang, N. S. Chang, P. J. Campagnola, C. Y. Dang and S. J. Chen, *Opt. Express*, 2012, **20**, 13669-13676.
- 8 W. S. Kuo, C. H. Lien, K. C. Cho, C. Y. Chang, C. Y. Lin, L. L. H. Huang, P. J. Campagnola, C. Y. Dong and S. J. Chen, *Opt. Express*, 2010, **18**, 27550-27559.
- 9 C. H. Lien, W. S. Kuo, K. C. Cho, C. Y. Lin, Y. D. Su, L. L. Huang, P. J. Campagnola, C. Y. Dong and S. J. Chen, *Opt. Express*, 2011, **19**, 6260-6268.
- 10 H. Wang, T. B. Huff, D. A. Zweifel, W. He, P. S. Low, A. Wei and J. X. Cheng, *Proc. Natl. Acad. Sci. USA*, 2005, **102**, 15752-15756.
- 11 G. Zhou and M. Gu, *Opt. Lett.*, 2006, **31**, 2783-2785.
- 12 C. Xu, W. Zipfel, J. B. Shear, R. M. Williams and W. W. Webb, *Proc. Natl. Acad. Sci. USA*, 1996, **93**, 10763-10786.
- 13 L. C. Cheng, N. G. Horton, K. Wang, S. J. Chen and C. Xu, *Biomed. Opt. Express*, 2014, **5**, 3427-3433.
- 14 C. Xu and W. W. Webb, *J. Opt. Soc. Am. B*, 1996, **13**, 481-491.
- 15 N. J. Durr, T. Larson, D. K. Smith, B. A. Korgel, K. Sokolov and A. Ben-Yakar, *Nano Lett.*, 2007, **7**, 941-945.
- 16 J. R. Akowicz, *3rd. Edition. Springer.*, 2010.
- 17 W. T. Chang, S. J. Chen, C. Y. Chang, Y. H. Liu, C. H. Chen, C. H. Yang, L. C. Chou, J. C. Chang, L. C. Cheng, W. S. Kuo and J. Y. Wang, *ACS Appl. Mater. Interfaces*, 2015, **7**, 17318-17329.
- 18 W. S. Kuo, S. M. Hwang, H. T. Sei, Y. C. Ku, L. F. Hsu, P. C. H. Hsieh and C. S. Yeh, *J. Chin. Chem. Soc.*, 2009, **56**, 940-948.
- 19 W. S. Kuo, Y. C. Ku, H. T. Sei, F. Y. Cheng and C. S. Yeh, *J. Chin. Chem. Soc.*, 2009, **56**, 923-934.
- 20 A. M. Rao, P. C. Eklund, S. Banbow, A. Thess and R. E. Smalley, *Science*, 1997, **388**, 257-259.
- 21 S. Park, N. Mohanty, J. W. Suk, A. Nagaraja, J. Q. R. D. Piner, W. Cai, V. Berry and R. S. Rouff, *Adv. Mater.*, 2010, **22**, 1736.
- 22 O. Carmel-Hare and G. Storz, *Annu. Rev. Microbiol.*, 2000, **54**, 439.
- 23 G. L. Ellman, *Arch. Biochem. Biophys.*, 1959, **82**, 70.
- 24 A. M. Rao, P. C. Eklund, S. Banbow, A. Thess and R. E. Smalley, *Science*, 1997, **388**, 257-259.

- 25 S. Zhu, J. Zhang, C. Qiao, S. Tang, Y. Li, W. Yuan, B. Li, L. Tian, F. Liu, R. Hu, H. Gao, H. Wei, H. Zhang, H. Sun and B. Yang, *Chem. Commun.*, 2011, **47**, 6858-6860.
- 26 C. T. Chien, S. S. Li, W. J. Lai, Y. C. Yeh, H. A. Chen, I. S. Chen, *Angew. Chem. Int. Ed.*, 2012, **51**, 6662-6666.
- 27 D. Y. Pan, J. C. Zhang, Z. Li and M. H. Wu, *Adv. Mater.*, 2010, **22**, 734-738.
- 28 J. Shen, Y. Zhu, C. Chen, X. Yang and C. F. Li, *Chem. Commun.*, 2011, **47**, 2580-2582.
- 29 Y. Li, Y. Hu, Y. Zhao, G. Shi, L. Deng, Y. Hou and L. Qu, *Adv. Mater.*, 2011, **23**, 776-780.
- 30 R. Liu, D. Wu, X. Feng and K. Müllen, *J. Am. Chem. Soc.*, 2011, **133**, 15221-15223.
- 31 L. Tang, R. Ji, X. Cao, J. Lin, H. Jiang, X. Li, K. S. Ten, C. M. Luk, S. Zeng, J. Hao and S. P. Lau, *ACS Nano*, 2012, **6**, 5102-5110.